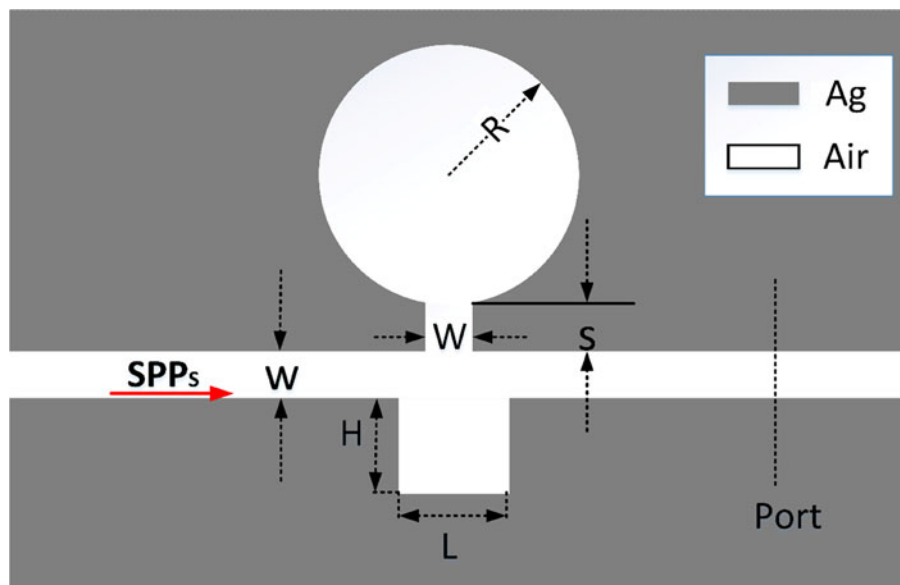


Ultrasharp Fano Resonances Based on the Circular Cavity Optimized by a Metallic Nanodisk

Volume 8, Number 6, December 2016

Yilin Wang
Shilei Li
Yunyun Zhang
Li Yu



DOI: 10.1109/JPHOT.2016.2628805
1943-0655 © 2016 IEEE

Ultrasharp Fano Resonances Based on the Circular Cavity Optimized by a Metallic Nanodisk

Yilin Wang, Shilei Li, Yunyun Zhang, and Li Yu

State Key Laboratory of Information Photonics and Optical Communications, Beijing
University of Posts and Telecommunications, Beijing 100876, China

DOI:10.1109/JPHOT.2016.2628805

1943-0655 © 2016 IEEE. Translations and content mining are permitted for academic research only.
Personal use is also permitted, but republication/redistribution requires IEEE permission.
See http://www.ieee.org/publications_standards/publications/rights/index.html for more information.

Manuscript received October 11, 2016; revised October 30, 2016; accepted November 10, 2016. Date of publication November 15, 2016; date of current version December 1, 2016. This work was supported in part by the Ministry of Science and Technology of China under Grant 2016YFA0301300; in part by the National Natural Science Foundation of China under Grant 11374041, Grant 11574035, and Grant 11404030; and in part by the Fund of State Key Laboratory of Information Photonics and Optical Communications, Beijing University of Posts and Telecommunications, PR China. Corresponding author: L. Yu (e-mail: yuliyuli@bupt.edu.cn).

Abstract: A compact structure is proposed to achieve double ultrasharp Fano profiles, which comprises with a metal-insulator-metal (MIM) bus waveguide coupled with a circular cavity and groove resonator. Simulation results show that these two sharp Fano profiles both originate from the interference between the circular cavity and the groove resonator. To optimize the Fano profiles, we introduce a metallic nanodisk in the middle of the circular cavity. The peak of the double Fano resonances can be independently tuned within a certain range by changing the radius of the nanodisk. We can utilize these characteristics to design devices with high performance, such as a highly efficient nanosensor with a sensitivity of ~ 1450 nm/RIU and a figure of merit (FOM) about $\sim 3.51 \times 10^4$ and a switch with an on/OFF contrast ratio of about 91 dB. Our structures may have promising applications in nanosensors, switches, and slow-light devices.

Index Terms: Surface plasmons, plasmonic waveguide, fano resonance, sensor.

1. Introduction

Fano resonance, which exhibits sharp and asymmetric spectral line shape, arises from the interference between a narrow discrete resonance and a broad continuum [1]. Different from the Lorentzian resonance, the Fano resonance possesses distinctly asymmetric line profile [2]. Due to its coherent sensitivity, a dramatic line shape shift of Fano resonance can be induced by a small change of the local environment [3]. Therefore, it shows great potential in the sensors, switches, slow light, and nonlinear areas [2], [4], [5]. In comparison with Fano resonance, electromagnetically induced transparency (EIT) is a quantum interference effect with a spectrally narrow optical enhanced transmission, which results from a coherent interaction between the atomic levels and the applied optical fields [6]. The theoretical analysis and experimental observations demonstrate that an optical phenomenon analogous to EIT can also occur in the coupled optical resonator systems [7]. Under certain conditions a Fano resonance can also be essentially regarded as the classical analogue of EIT. Such as strongly contrasting resonance line widths and appropriate resonance amplitudes [8]. Recently, some nanoscale photonic devices for high integration emerged, which utilize the unique properties

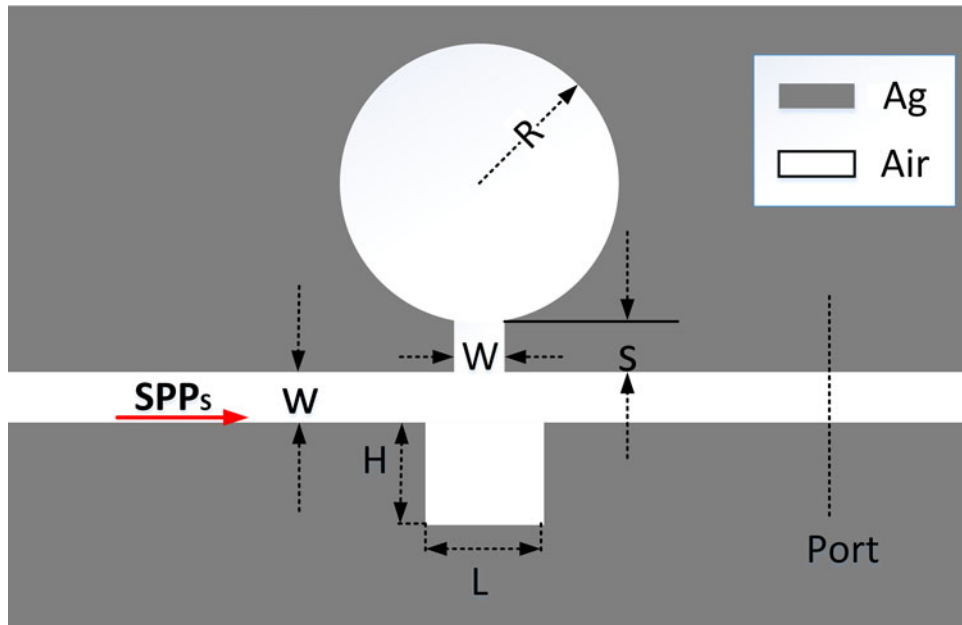


Fig. 1. Schematic diagram of the proposed plasmonic structure based on MIM waveguide.

of surface plasmon polaritons (SPPs) [9]–[12]. SPPs have the stand potential to overcome the diffraction limit and confine light in sub-wavelength dimensions. Various plasmonic systems have been designed to achieve the Fano profiles [13]–[16]. Most Fano responses can be designed by asymmetric plasmonic structures, such as the symmetry-breaking plasmonic nanocavity [17], non-concentric ring or disk cavity [18], or nanodisk with a defect [19]. As an important plasmonic waveguide, the metal-insulator-metal (MIM) waveguide, which has wide applications in deep subwavelength optical devices, has attracted much attention in recent years [20].

In this paper, we employ the MIM structure to realize two ultra-sharp and asymmetric spectral profiles which have a great sensitivity and a large figure of merit (FOM). In our proposed plasmonic structure, Fano resonances can be obtained by comprising a MIM waveguide coupled with a simple groove and a circular cavity. In this structure, the circular cavity is behaving as a Fabry-perot (F-P) resonator which provides a narrow discrete resonance, while the groove resonator provides a broad continue transmission profile. The combination of them gives rise to the Fano resonances. In order to obtain Fano profiles with better properties, we introduce a metallic nanodisk in the middle of the circular cavity. Simulation results show that the new structure can serve as an excellent sensor with a sensitivity of 1450 nm/RIU and an FOM of $\sim 3.51 \times 10^4$. It can also be used in nanoscale optical switching which exhibits an on/off contrast ratio of about 91dB. When we adjust the radius of the nanodisk, an interesting phenomenon can be found. That is, one of the resonant wavelengths can be tuned, while the other almost remains unchanged. Therefore, our structure find a new way to tune resonant wavelengths in circular cavity.

2. Sharp Fano Resonances Induced by Circular Cavity Coupled With Groove Resonator

Fig. 1 schematically shows the MIM waveguide coupled with a circular cavity and a groove resonator which placed in both sides of the bus waveguide. This structure is a two-dimensional model, and the gray and white parts denote Ag ($\varepsilon_m(\omega)$) and Air ($\varepsilon_d = 1.0$), respectively. The width of the bus is denoted as W . The length and height of the groove are L and H . In the simulations, the parameters are set as follows: $R = 370$ nm, $S = 100$ nm, $W = 50$ nm, $L = 200$ nm, and $H = 225$ nm, and the sizes of the groove are fixed throughout this paper.

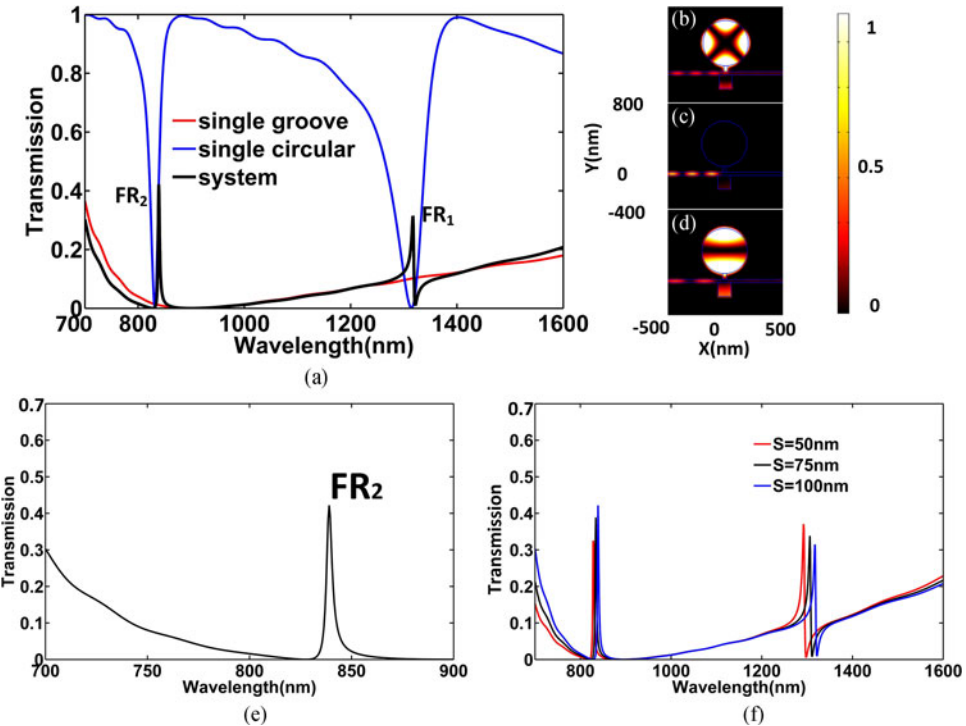


Fig. 2. (a) Transmission spectra of the single circular cavity (blue line), single groove resonator (red line), and the system when $R = 370$ nm. The corresponding $|H_z|^2$ field distributions with wavelengths of (b) 839 nm (FR₂ peak), (c) 900 nm (FR₂ valley), and (d) 1317 nm (FR₁ peak) exhibit different transmission features. (e) Enlarged view of FR₂ when zoom in the scale from 700 nm to 900 nm. (f) Transmission spectra with different length (S) of the gap.

To investigate the optical responses of the proposed structure, its transmission spectra are numerically calculated using the finite element method (FEM) of COMSOL Multiphysics. The transmitted light is collected from the right side of the bus waveguide, and the transmission is defined as $T = p_{out}/p_{in}$, where p_{out} and p_{in} stand for the power flows of the Port (obtained by integrating the Poynting vector over the channel cross-section) with structures(circular cavity and groove resonator) and without structures, respectively [20], [21]. The permittivity of Ag can be determined by the well-known Drude model: $\varepsilon_m(\omega) = \varepsilon_\infty - \omega_p^2/[\omega(\omega + i\gamma)]$, where the parameters for silver can be set as $\varepsilon_\infty = 3.7$, $\omega_p = 9.1$ ev and $\gamma = 0.018$ ev [22], which corresponds to the experimental optical constant of silver well [23].

First, we simulate the transmission characteristics of our proposed structure. When the circular cavity is set as $R = 370$ nm and the transmission spectra, which consists of two sharp Fano resonances, is shown in Fig. 2(a), we called the right Fano resonance FR₁, while the left Fano resonance is FR₂. From This, we find the single circular cavity exhibits a broadband transmission spectra with nearly symmetric Lorentzian-like line-shapes, while the groove resonator provides a broad spectrum, and the sharp and symmetric spectra FR₁, usually termed Fano profiles, result from the coupling of the narrow discrete state (circular cavity) and the continuum (groove resonator). The origin of FR₂ can also be explained by this mechanism. For a clearer look of FR₂, the enlarged view is shown in Fig. 2(e). To further investigate the origin of this two mode, the field distributions of $|H_z|^2$ at the incident wavelength of $\lambda = 839$ nm and $\lambda = 1317$ nm are depicted in Fig. 2(b) and (d), corresponding to FR₂ peak and FR₁ peak, respectively. The underlying principle of the Fano resonances can be divided into two types which are phase-coupling and near-field coupling mechanisms [24]. The Fano resonances in our structure originate from phase-coupling mechanism. As the field distributions shows, near the resonant wavelengths, the SPPs can be highly reflected by the circular resonators, acting as a high reflector. Thus, the SPPs can be reflected up and

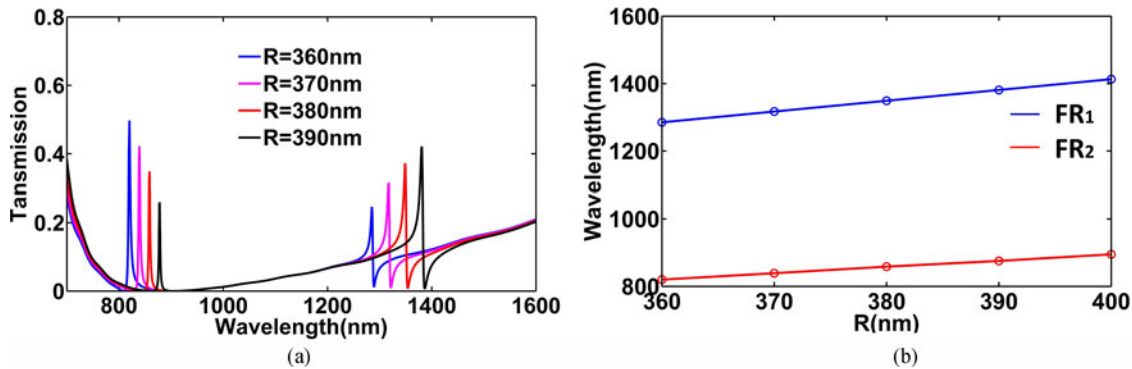


Fig. 3. (a) Transmission spectra with different radius of the circular cavity(R). (b) Relationship between the peak positions of the FR₁, FR₂, and R.

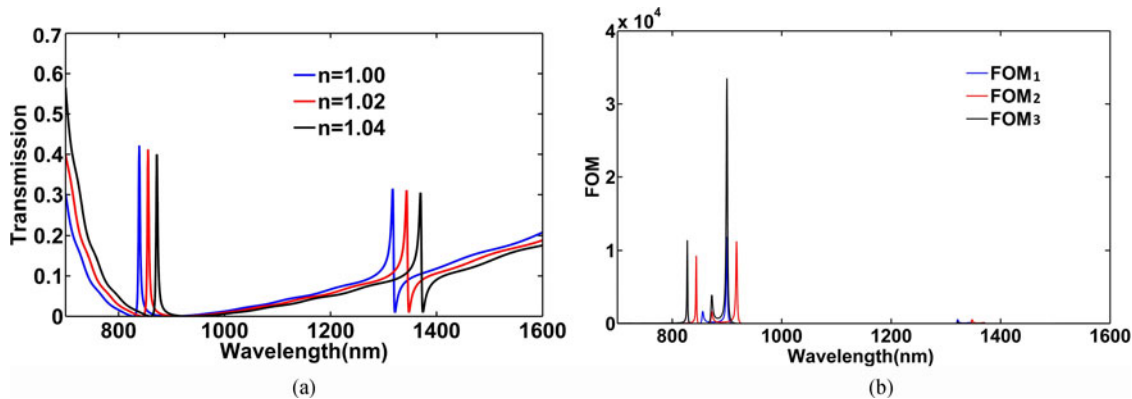


Fig. 4. (a) Transmission spectra for different refractive index. (b) Calculated FOM at different wavelengths.

down off the two resonators through the gap with high reflectivity, constructing a new Fabry–Perot (FP) resonator in the plasmonic system. It can be confirmed when we increase the gap length (S) which can reflect the phase value of the new FP, the resonant wavelengths exhibit redshifts as shown in Fig. 2(f). The distribution $|H_z|^2$ at 1317 nm shows the interference between $n = 1$ order of circular resonance and the groove resonance, while the FR₂ is the result of $n = 2$ order of circular resonance and the groove resonance. In addition, there exists no excitation of resonant mode when the wavelength is 900 nm, as shown in Fig. 2(c).

Successively, we investigate the influence of the radius of the circular cavity (R) on the transmission spectra and Fig. 3(a) shows the transmission response corresponding to different R. As a result, the resonant wavelengths have a red-shift with increasing of the radius. We also find that the transmission of FR₁ increases while FR₂ decreases with the increasing of radius. Fig. 3(b) reveals that the wavelength-shifts of the resonant FR₁ and FR₂ almost have approximately linear relations with the radius of circular cavity. With the increase of R by 10 nm, the FR₁ and FR₂ have redshifts about 32 nm and 20 nm, respectively. Therefore, we can get different resonant wavelengths by adjusting R according to this relationship.

Our proposed Fano resonance system has great potential as a refractive index sensor due to its sharp asymmetric spectra [25]. Therefore, we studied the transmission spectra of the structure with different refractive index materials and the results are shown in Fig. 4(a). With increasing of n from 1 to 1.04, the peak positions of FR₁ and FR₂ are both red shifts and show the nearly linear relationships. The sensitivity (nm/RIU) is defined as the shift in the resonance wavelength per unit change of the refractive index. The sensitivity of our structure is about 1350 nm/RIU for FR₁ and

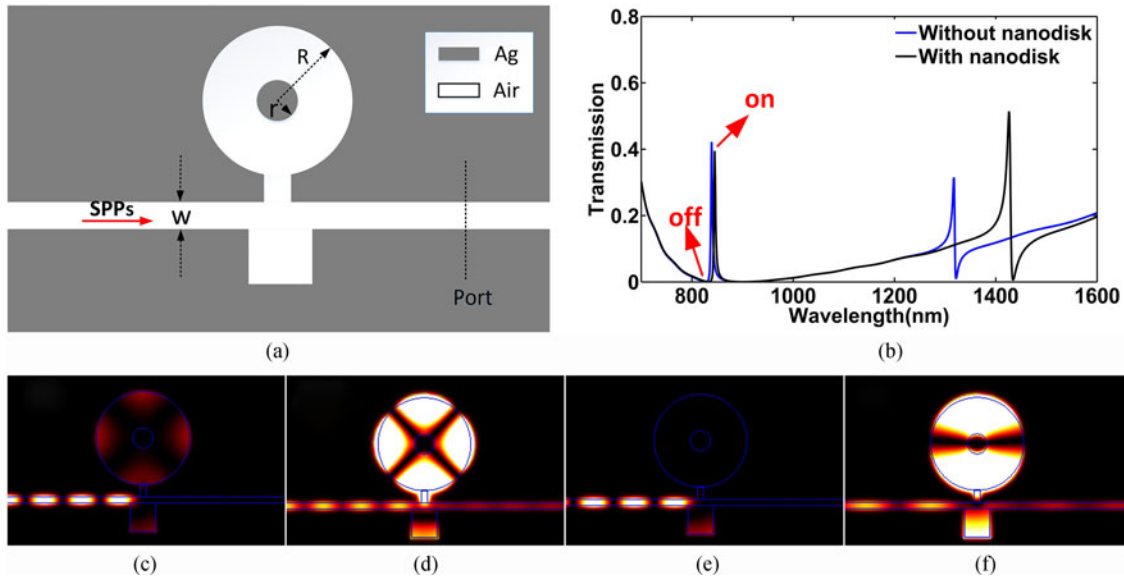


Fig. 5. (a) Schematic diagram of the improved plasmonic structure by adding a nanodisk with radius r . (b) Transmission spectra with (blue line) and without (black line) nanodisk when $r = 80$ nm. The corresponding $|H_z|^2$ field distributions with wavelengths of (c) 833 nm (left valley of FR_2), (d) 845 nm (FR_2 peak), (e) 900 nm (right valley of FR_2), and (f) 1426 nm (FR_1 peak) exhibit different transmission features.

800 nm/RIU for FR_2 , which is excellent compared with those in [26] and [27]. Moreover, FOM as a key parameter is widely used to evaluate the performance of the double Fano resonances, which is defined as $FOM = \Delta T / (T \Delta n)$ [28], [29], where $\Delta T / \Delta n$ denotes the transmission change at the fixed wavelength induced by a refractive index change. To make more general calculations, we define $FOM_1 = (T_{n=1.02} - T_{n=1.00}) / (T_{n=1.00} \Delta n)$, $FOM_2 = (T_{n=1.04} - T_{n=1.02}) / (T_{n=1.02} \Delta n)$ and $FOM_3 = (T_{n=1.04} - T_{n=1.00}) / (T_{n=1.00} \Delta n)$, respectively, and the calculated results are shown in Fig. 4(b). FOM_3 can reach 3.35×10^4 at $\lambda_0 = 900$ nm, which is due to the sharp asymmetric Fano line-shape with ultra-low transmittance at this wavelength. This value is much higher than that of the plasmonic sensors [26], [29].

3. Adding a Nanodisk in the Circular Cavity

To further study the above plasmonic system, we introduce a metallic nanodisk in the middle of the circular cavity as shown in Fig. 5(a). The same method is used as mentioned above to study the new structure, and the transmission spectra are depicted in Fig. 5(b) by black line. Clearly, we can see that the peak value of FR_1 is significantly improved and accompanied by a redshift, but the FR_2 almost remains unchanged. This phenomenon is easy to understand. From the different field distributions of $|H_z|^2$ at left valley of FR_2 in Fig. 5(c) and FR_2 peak wavelength in Fig. 5(d), we can see that the field distributions of FR_2 mainly concentrate in the periphery of the circular, so by introduce a nanodisk with right size in the center hardly changes the properties of FR_2 . Meanwhile, at the FR_1 peak wavelength shown in Fig. 5(f), the nanodisk with $r = 80$ nm greatly affects the field distribution compared with circular resonance in Fig. 2(d). Thus, the properties of FR_1 exhibit significant changes.

Through the above analysis, we can tune more flexibly of the peak position of FR_1 and FR_2 . When we change the radius of the nanodisk (r) from 0-80 nm while keeping the R as 370 nm, one fantastic phenomenon occurs which is shown in Fig. 6(a). That is, the peak position of FR_2 remains unchanged, while the FR_1 changes nonlinearly, and the relationship is shown in Fig. 6(b). This is due to the differences between electromagnetic fields of FR_1 and FR_2 , as explained in the previous

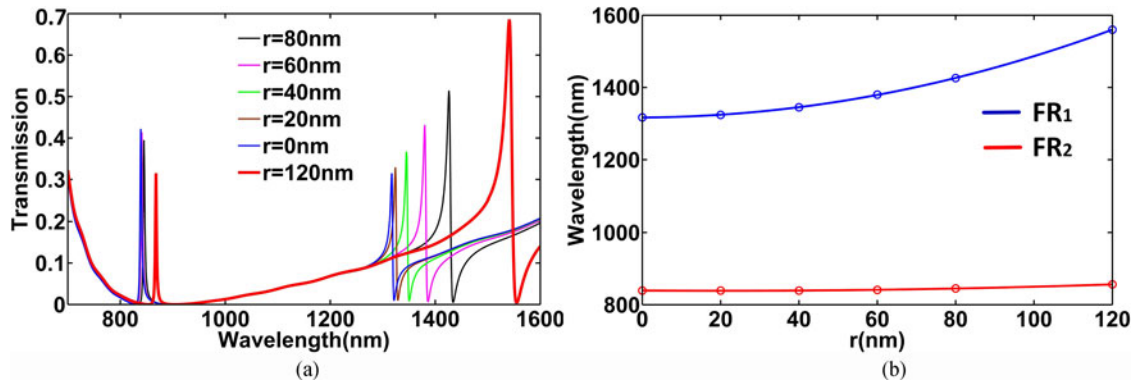


Fig. 6. (a) Transmission spectra with different radius of the nanodisk (r). (b) Relationship between the peak position of the double Fano resonances and r .

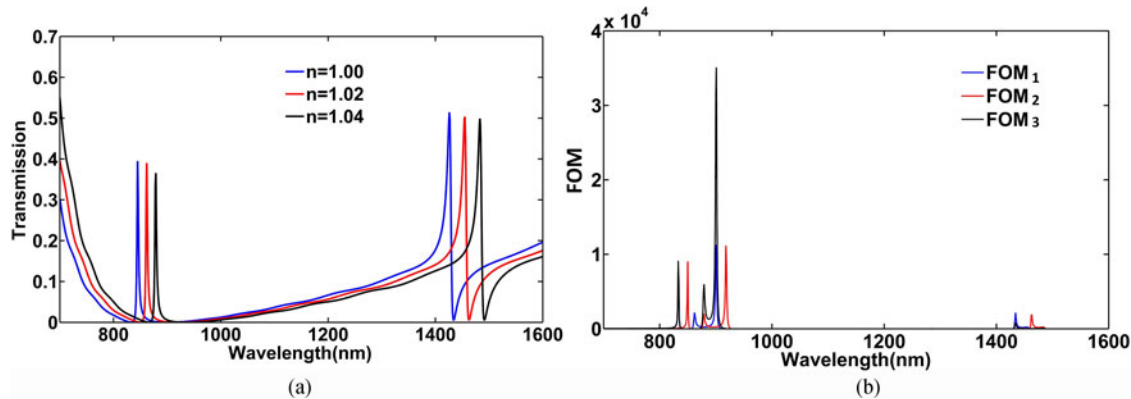


Fig. 7. (a) Transmission spectra for different refractive index. (b) The calculated FOM at different wavelengths.

paragraph. It also can be confirmed When r is large enough, like Fig. 6(a), in the case when $r = 120$ nm (red line), FR₂ presents an obvious movement. We should note that when $r = 0$ nm (blue line) which denotes the circular cavity, FR₁ transport properties deteriorate, which is one of the reasons why we adding a nanodisk in the circular cavity.

Successively, we investigate the application as the sensor based on the optimized plasmonic structure. Because of the short wavelength change which is only 8 nm for FR₁ from resonant peak to the valley, the transmission spectra of the structure is very sensitive to the index variations of surrounding medium for the structure embedded in the cavity. Therefore, we investigate the transmission spectra of the structure with different refractive index materials and the results are shown in Fig. 7(a). With increasing of n from 1 to 1.04, the peak positions of FR₁ and FR₂ are also both red shifts and show the nearly linear relationships. The sensitivity is about 1450 nm/RIU for FR₁, which is excellent compared with the value of circular cavity and those in the references [26], [27]. Moreover, the calculated results of our new structure is shown in Fig. 5(b). The values of FOM₃ is as high as 3.51×10^4 at $\lambda_0 = 901$ nm which is the valley of FR₂. This high FOM is due to the sharp asymmetric Fano line-shape with ultra-low transmittance at this wavelength. Here, FOM is also improved compared with the value of circular cavity and is much higher than that of the plasmonic sensors [26], [29].

Optical switch is one of the core devices in optical information processing and optical communication network [30]–[32]. The sharp Fano lines presented in this paper are ideal for designing optical switches. The transmission can drop sharply from peak to the valley of the spectrum as denoted by

the black line in Fig. 5, and the distance between them is only about 12 nm for FR₂. Such a short wavelength change can make the optical switch quickly switch between “on” and “off” state. We can clearly see the differences of the $|H_z|^2$ field distributions between “on” and “off” states which are shown in the pictures of Fig. 5(d) and (c). Another important indicator of the optical switch is on/off contrast ratio, which can be determined by $Ratio = 10 \times \log_{10} T_{\max}/T_{\min}$ [33], where T_{\max} and T_{\min} stand for the transmission of the peak and valley, respectively. Using the above formula, we can get the on/off contrast ratio of our switch is about 91 dB, which is significantly high than previous report [33], [34]. In the practical applications, we can employ graphene to get a graphene-integrated FP to tune the switch more flexibly. As mentioned in [35], the authors employ two graphene ribbon arrays (GRAs) to dynamically tune the frequency window.

4. Conclusion

In summary, ultra-sharp double Fano resonances in an MIM waveguide coupled with groove and circular cavity are numerically predicted and properties of them are greatly improved by adding a nanodisk in the middle of the circular cavity. One of the Fano lines has an only 8 nm wavelength shift from the resonant peak to the valley, and the double Fano profiles and the resonant wavelengths can be easily tuned by changing the radius of the nanodisk. Based on the above unique features, a nano-sensor was designed, which yielded a sensitivity of ~ 1450 nm/RIU and an FOM of $\sim 3.51 \times 10^4$ at $\lambda_0 = 901$ nm. An optical switch was also investigated based on the Fano resonances with an on/off contrast ratio about 91dB. The utilization of the ultra-sharp Fano resonances in the MIM waveguide has a great potential in designing ultra-high performance plasmonic devices.

References

- [1] L. F. Niu *et al.*, “Fano resonance in dual-disk ring plasmonic nanostructures,” *Opt. Exp.*, vol. 19, no. 23, pp. 22974–22981, Nov. 2011.
- [2] A. Miroshnichenko, S. Flach, and Y. Kivshar, “Fano resonances in nanoscale structures,” *Rev. Mod. Phys.*, vol. 82, no. 3, pp. 2257–2298, Aug. 2010.
- [3] Z. D. Zhang, H. Y. Wang, and Z. Y. Zhang, “Fano resonance in a gear-shaped nanocavity of the metal–insulator–metal waveguide,” *Plasmonics*, vol. 8, no. 2, pp. 797–801, Jun. 2013.
- [4] K. Wen *et al.*, “Fano resonance with ultra-high figure of merits based on plasmonic metal-insulator-metal waveguide,” *Plasmonics*, vol. 10, no. 1, pp. 27–32, Feb. 2015.
- [5] N. Verellen *et al.*, “Fano resonances in individual coherent plasmonic nanocavities,” *Nano Lett.*, vol. 9, no. 4, pp. 1663–1667, Apr. 2009.
- [6] K. J. Boller, A. Imamoglu, and S. E. Harris, “Observation of electromagnetically induced transparency,” *Phys. Rev. Lett.*, vol. 66, no. 20, pp. 2593–2596, May 1991.
- [7] D. D. Smith *et al.*, “Coupled-resonator-induced transparency,” *Phys. Rev. A*, vol. 69, no. 6, Jun. 2004, Art. no. 063804.
- [8] B. Luk'yanchuk *et al.*, “The Fano resonance in plasmonic nanostructures and metamaterials,” *Nature Mater.*, vol. 9, no. 9, pp. 707–715, Sep. 2010.
- [9] S. Enoch, R. Quidant, and G. Badenes, “Optical sensing based on plasmon coupling in nanoparticle arrays,” *Opt. Exp.*, vol. 12, no. 15, pp. 3422–3427, Jul. 2004.
- [10] H. Kim, J. Park, and B. Lee, “Tunable directional beaming from subwavelength metal slits with metal-dielectric composite surface gratings,” *Opt. Lett.*, vol. 34, no. 17, pp. 2569–2571, Sep. 2009.
- [11] V. F. Nezhad, S. Abaslou, and M. S. Abrishamian, “Plasmonic band-stop filter with asymmetric rectangular ring for WDM networks,” *J. Opt.*, vol. 15, no. 5, Apr. 2013, Art. no. 055007.
- [12] Z. Chai *et al.*, “Ultracompact chip-integrated electromagnetically induced transparency in a single plasmonic composite nanocavity,” *Adv. Opt. Mater.*, vol. 2, no. 4, pp. 320–324, Apr. 2014.
- [13] J. W. Qi *et al.*, “Independently tunable double Fano resonances in asymmetric MIM waveguide structure,” *Opt. Exp.*, vol. 22, no. 12, pp. 14688–14695, Jun. 2014.
- [14] B. Luk'yanchuk *et al.*, “The Fano resonance in plasmonic nanostructures and metamaterials,” *Nat. Mater.*, vol. 9, no. 9, pp. 707–715, Sep. 2010.
- [15] J. B. Lassiter *et al.*, “Fano resonances in plasmonic nanoclusters: geometrical and chemical tunability,” *Nano Lett.*, vol. 10, no. 8, pp. 3184–3189, Aug. 2010.
- [16] Z. Chen and L. Yu, “Multiple fano resonances based on different waveguide modes in a symmetry breaking plasmonic system,” *IEEE Photon. J.*, vol. 6, no. 6, Nov. 2014, Art. no. 4802208.
- [17] F. Hao *et al.*, “Symmetry breaking in plasmonic nanocavities: subradiant LSPR sensing and a tunable Fano resonance,” *Nano Lett.*, vol. 8, no. 11, pp. 3983–3988, Nov. 2008.
- [18] F. Hao *et al.*, “Tunability of subradiant dipolar and fano-type plasmon resonances in metallic ring/disk cavities: Implications for nanoscale optical sensing,” *ACS Nano*, vol. 3, no. 3, pp. 643–652, Mar. 2009.

- [19] Z. Fang *et al.*, "Removing a wedge from a metallic nanodisk reveals a fano resonance," *Nano Lett.*, vol. 11, no. 10, pp. 4475–4479, Oct. 2011.
- [20] Z. Chen *et al.*, "A refractive index nanosensor based on fano resonance in the plasmonic waveguide system," *IEEE Photon. Technol. Lett.*, vol. 27, no. 16, pp. 1695–1698, Aug. 2015.
- [21] Z. Chen *et al.*, "Spectral splitting based on electromagnetically induced transparency in plasmonic waveguide resonator system," *Plasmonics*, vol. 10, no. 3, pp. 721–727, Jun. 2015.
- [22] Z. Han, E. Forsberg, and S. He, "Surface plasmon bragg gratings formed in metal-insulator-metal waveguides," *IEEE Photon. Technol. Lett.*, vol. 19, no. 2, pp. 91–93, Jan. 2007.
- [23] P. B. Johnson and R. W. Christy, "Optical constants of the noble metals," *Phys. Rev. B*, vol. 6, no. 12, pp. 4370–4379, Dec. 1972.
- [24] C. Zeng, Y. Cui, and X. Liu, "Tunable multiple phase-coupled plasmon-induced transparencies in graphene metamaterials," *Opt. Exp.*, vol. 23, no. 1, pp. 545–551, Jan. 2015.
- [25] Z. Chen *et al.*, "Sharp asymmetric line shapes in a plasmonic waveguide system and its application in nanosensor," *J. Lightw. Technol.*, vol. 33, no. 15, pp. 3250–3253, Aug. 2015.
- [26] H. Lu, X. M. Liu, D. Mao, and G. X. Wang, "Plasmonic nanosensor based on Fano resonance in waveguide-coupled resonators," *Opt. Lett.*, vol. 37, no. 18, pp. 3780–3782, Sep. 2012.
- [27] N. Liu *et al.*, "Planar metamaterial analogue of electromagnetically induced transparency for plasmonic sensing," *Nano Lett.*, vol. 10, no. 4, pp. 1103–1107, Apr. 2010.
- [28] J. Becker, A. Trugler, A. Jakab, U. Hohenester, and C. Sonnichsen, "The optimal aspect ratio of gold nanorods for plasmonic bio-sensing," *Plasmonics*, vol. 5, no. 2, pp. 161–167, Jun. 2010.
- [29] R. Ameling *et al.*, "Cavity-enhanced localized plasmon resonance sensing," *Appl. Phys. Lett.*, vol. 97, no. 25, Dec. 2010, Art. no. 253116.
- [30] K. Nozaki *et al.*, "Ultralow-energy and high-contrast all-optical switch involving Fano resonance based on coupled photonic crystal nanocavities," *Opt. Exp.*, vol. 21, no. 10, pp. 11877–11888, May 2013.
- [31] X. Zhang *et al.*, "Tunable ultrafast optical switching via waveguided gold nanowires," *Adv. Mater.*, vol. 20, no. 23, pp. 4455–4459, Dec. 2008.
- [32] R. A. Pala *et al.*, "A nonvolatile plasmonic switch employing photochromic molecules," *Nano Lett.*, vol. 8, no. 5, pp. 1506–1510, May 2008.
- [33] J. Chen, Z. Li, X. Zhang, J. H. Xiao, and Q. H. Gong, "Submicron bidirectional all-optical plasmonic switches," *Sci. Rep.*, vol. 3, Mar. 2013, Art. no. 1451.
- [34] J. Chen *et al.*, "Highly efficient all-optical control of surface-plasmon-polariton generation based on a compact asymmetric single slit," *Nano Lett.*, vol. 11, no. 7, pp. 2933–2937, Jul. 2011.
- [35] C. Zeng, J. Guo, and X. Liu, "High-contrast electro-optic modulation of spatial light induced by graphene-integrated Fabry-Pérot microcavity," *Appl. Phys. Lett.*, vol. 105, no. 12, Sep. 2014, Art. no. 121103.